Int J Biometeorol (2015) 59:205–216
DOI 10.1007/s00484-014-0836-2

ORIGINAL PAPER

Dynamic modeling of human thermal comfort after the transition from an indoor to an outdoor hot environment

George Katavoutas · Helena A. Flocas · Andreas Matzarakis

Received: 26 June 2013 / Revised: 14 April 2014 / Accepted: 14 April 2014 / Published online: 15 May 2014

Abstract Thermal comfort under non-steady-state conditions primarily deals with rapid environmental transients and significant alterations of the meteorological conditions, activity, or clothing pattern within the time scale of some minutes. In such cases, thermal history plays an important role in respect to time, and thus, a dynamic approach is appropriate. The present study aims to investigate the dynamic thermal adaptation process of a human individual, after his transition from a typical indoor climate to an outdoor hot environment. Three scenarios of thermal transients have been considered for a range of hot outdoor environmental conditions, employing the dynamic two-node IMEM model. The differences among them concern the radiation field, the activity level, and the body position. The temporal pattern of body temperatures as well as the range of skin wettedness and of water loss have been investigated and compared among the scenarios and the environmental conditions considered. The structure and the temporal course of human energy fluxes as well as the identification of the contribution of body temperatures to energy fluxes have also been studied and compared. In general, the simulation results indicate that the response of a person, coming from the same neutral indoor climate, varies depending on the scenario followed by the individual while being outdoors. The combination of radiation field (shade or not) with the kind of activity (sitting or walking) and the outdoor conditions differentiates significantly the thermal state of the human body. Therefore, 75 % of the skin wettedness values do not exceed the thermal comfort limit at rest for a sitting individual under the shade. This percentage decreases dramatically, less than 25 %, under direct solar radiation and exceeds 75 % for a walking person under direct solar radiation.

Keywords Thermal comfort · Non-steady-state conditions · IMEM · Body temperatures · Human energy fluxes · Thermal transients

G. Katavoutas (✉) · H. A. Flocas
Department of Environmental Physics-Meteorology, Faculty of Physics, University Campus-Zografou, University of Athens, 15784 Athens, Greece
e-mail: geokat@phys.uoa.gr

A. Matzarakis
Chair of Meteorology and Climatology, Albert-Ludwigs-University Freiburg, Werthmannstrasse 10, D-79085 Freiburg, Germany

Introduction

In the developed world, people spend less than 20 % of their time outdoors and about one-third of the day outside the buildings (Leech et al. 2002; Brasche and Bischof 2005). The outdoor parameters can be considerably more diverse in the outdoor thermal environment, with stronger variation than in the indoor setting. Therefore, people are exposed to a variety of outdoor microclimates, which are generally assumed to be beyond architectural and mechanical control (Spagnolo and de Dear 2003). The combination of this relatively short residence time with the exposure to a variety of outdoor microclimates has as a result that people staying outdoors hardly reach thermal steady-state conditions (Höppe 2002). In a study based on thermal comfort votes, along courses in transient semi-outdoor (dynamic) conditions in transitional spaces (Chun and Tamura 2005), the authors state "in real transitional spaces, people experience temperature change in a very short term and continuously, not once in 1 or 2 h like in the laboratory. There is no steady state when people are walking in transitional spaces".

Non-steady-state thermal comfort primarily deals with rapid environmental transients and significant alterations of the meteorological conditions, activity, or clothing pattern within the time scale of some minutes (de Dear et al. 1993; Höppe 1993; Höppe 1997). In such cases, thermal history plays an

important role in respect to time, and thus, a dynamic approach is appropriate.

In the past 40 years, a number of models have been developed, based on the energy balance equations for the human body and the energy exchange mechanisms. These models vary, from steady-state to dynamic models and from one-node to two-node to multi-node and multi-element models. One of the most well-known steady-state models is the Fanger's one-dimensional model (Fanger 1972). This model provides a comfort index, and it is best used to predict the qualitative behavior of the body and is of less value in predicting thermal response quantitatively (Schappeler 2011), since the thermal responses predicted are based on formulas obtained from comfort conditions (Höppe 1993). Another steady-state but two-node model is the MEMI model (Höppe 1984; Mayer and Höppe 1987; Höppe 1999). This model takes into account the thermoregulatory processes and can be employed in order to predict the quantitative and qualitative behavior of the human body in a simulated environment under steady-state conditions.

One of the most well-known two-node transient models is the Gagge's model, also known as the Pierce's model (Gagge et al. 1971). A model like this divides the body into two concentric shells, where the outer shell represents the skin layer and the interior shell represents internal organs, bones, muscles, and subcutaneous tissue. Höppe (1989, 1993) presented the dynamic two-node IMEM model. As a two-node model, IMEM is a lumped parameter model. This model takes into account the thermoregulatory processes, like the constriction or dilation of peripheral blood vessels, the physiological sweat rate and the production of energy by shivering, and certain parameters of the Gagge's two-node transient model. The main differences from the Gagge's model are the way that the physiological sweat rate is modeled and the separate computation of energy fluxes from clothed and unclothed segments of the body surface. The German VDI guideline includes the IMEM model for the evaluation of the thermal component of the bioclimate (VDI 1998). Recently, Zolfaghari and Maerefat (2010) presented a simplified bioheat model for transient environments based on the Gagge's two-node model. A new approach to apply the Pierce two-node model for individual body parts has also been formulated (Foda and Sirén 2011).

Multi-node and multi-element models divide the entire body into more than two concentric shells and into several elements representing body parts, respectively (e.g., Stolwijk 1971; Huizenga et al. 2001; Tanabe et al. 2002; Fiala et al. 2001; Yi et al. 2004; Al-Othmani et al. 2008).

From the perspective of dynamic modeling in the field of practical applications, Höppe (1997) presented an after entry into a sauna bath simulation, employing the dynamic two-node IMEM model, studying the temporal course of skin wettedness and mean skin temperature. According to simulations based on the same model, steady-state of mean skin and body core temperatures is reached after half and 1 h, respectively, for a person leaving a neutral indoor climate to the outdoor hot environment (Höppe 2002). On the contrary, simulations have shown that under cold outdoor conditions, thermal steady-state is never reached. Further, Höppe (2002) also studied the temporal course of body temperatures for a pedestrian coming from a shaded area to a sunny street canyon. A modified Pierce two-node model was implemented by Chen and Ng (2011, 2012) in order to assess pedestrian's thermal comfort conditions and sufficiently depict pedestrian's dynamic thermal adaptation process. The dynamic two-node IMEM model was also employed in order to investigate the thermophysiological parameters and the human energy fluxes for a person leaving an indoor environment and seating under tree shade conditions, during hot summer days (Katavoutas et al. 2012).

Multi-node and multi-element models can predict with good accuracy, but these models are the most complicated and especially the multi-element models require the knowledge of many geometric properties of the human body for calculation (Yi et al. 2004). Although the good accuracy is a desirable target, the simplicity is needed in order to enhance the simulation time in the field of practical applications.

In the present study, the dynamic two-node IMEM model has been employed in order to simulate the effects of the thermal environment on the human body in a thermophysiologically significant way, under non-steady-state conditions. This study aims to investigate the dynamic thermal adaptation process of a human individual, after his transition from a typical indoor climate to an outdoor hot environment. Three scenarios of thermal transients have been considered for a range of hot outdoor environmental conditions. The differences among them concern the radiation field, the activity level, and the body position. The thermal quantities of the body, i.e., mean skin temperature, core temperature, skin wettedness, and water loss as well as the human energy fluxes has been studied among the scenarios and the environmental conditions considered.

Materials and methods

Instationary Munich Energy Balance Model

The Instationary Munich Energy Balance Model (IMEM) is a dynamic two-node model in which the storage flow of sensible energy in the body tissue is considered in order to simulate the changes in the body temperatures (Höppe 1989, 1993). The model is based on a system of three fundamental

equations. The first one is the energy balance equation for the human body:

$$H + C + \mathrm{RN} + E_{\mathrm{D}} + E_{\mathrm{sw}} + E_{\mathrm{Re}} = S = c_{\mathrm{k}} \cdot \mathrm{GE} \cdot (\mathrm{dT_M}/\mathrm{dt}) \quad (1)$$

where H is the internal energy production (in W), C is the convective energy flux (in W), RN is the radiative energy flux (in W), E_{D} is the energy flux by skin diffusion (in W), E_{sw} is the energy flux due to evaporation of sweat (in W), E_{Re} is the sum of energy fluxes for heating and humidifying the inspired air (in W), S is the storage flow of sensible energy in the body tissue (in W), c_{k} is the specific heat of body (in $\mathrm{J\,kg^{-1}\,K^{-1}}$), GE is the body mass (in kg), T_{M} is the mean body temperature (in °C), and t is the time (in s).

The second equation is the energy flux from the body core to the skin surface (F_{cs}, in W):

$$F_{\mathrm{cs}} = v_{\mathrm{b}} \cdot \rho_{\mathrm{b}} \cdot c_{\mathrm{b}} \cdot A_{\mathrm{Du}} \cdot (T_{\mathrm{c}} - T_{\mathrm{sk}}) \quad (2)$$

where v_{b} is the blood flow from the core to the skin (in $\mathrm{l\,s^{-1}\,m^{-2}}$, depending on the mean skin and core temperatures), ρ_{b} is the density of blood (in $\mathrm{kg\,l^{-1}}$), c_{b} is the specific heat of blood ($\mathrm{WsK^{-1}\,kg^{-1}}$), A_{Du} is the surface area of the skin (in $\mathrm{m^2}$), T_{c} is the body core temperature (in °C), and T_{sk} is the mean skin temperature (in °C).

The third equation is the energy flux from the skin surface through the clothing layer to the clothing surface (F_{sc}, in W):

$$F_{\mathrm{sc}} = (A_{\mathrm{Be}}/I_{\mathrm{cl}}) \cdot (T_{\mathrm{sk}} - T_{\mathrm{cl}}) \quad (3)$$

where I_{cl} is the heat resistance of the clothing (in $\mathrm{m^2\,KW^{-1}}$), A_{Be} is the surface area of the clothed body (in $\mathrm{m^2}$), and T_{cl} is the clothing surface temperature (in °C). Taking into consideration the assumption that the clothing layer has no heat capacity, the F_{sc} has to be equal to the sum of convective and radiative energy fluxes.

Since certain segments of the human body are clothed and others are unclothed, the total body surface is divided in a covered and an uncovered surface. Therefore, the energy fluxes are evaluated separately from parts of the body that are covered or uncovered by clothing.

The onset of sweating is triggered mainly by the core temperature, but also high skin temperature values can cause sweat secretion. Therefore, the sweat rate (SW, in $\mathrm{kg\,s^{-1}}$) is modeled as a function of the mean skin and body core temperatures:

$$\mathrm{SW} = 8.47 \cdot 10^{-5} \cdot ((0.1 \cdot T_{\mathrm{sk}} + 0.9 \cdot T_{\mathrm{c}}) - 36.6) \cdot A_{\mathrm{Du}} \quad (4)$$

The energy production by shivering is modeled as a function of the mean skin and body core temperatures, where the deviations terms are set to zero if they became negative:

$$M_{\mathrm{shiv}} = 19.4 \cdot (34.0 - T_{\mathrm{sk}}) \cdot (37.0 - T_{\mathrm{c}}) \cdot A_{\mathrm{Du}} \quad (5)$$

The sweat rate is an entirely physiological parameter, which is not necessarily representative of the evaporative energy loss of sweat. The energy loss by evaporation of sweat depends on both the ambient conditions and the so-called potential evaporation from the body. The potential evaporation of sweat is the maximum evaporation under the certain ambient conditions. Consequently, when the amount of sweat produced is lower than the potentially evaporating amount of sweat, then all the produced sweat will evaporate, and the corresponding evaporative energy loss can be quantified by

$$E_{\mathrm{sw}} = \mathrm{SW} \cdot r \quad (6)$$

where r is the vaporization heat of water (in $\mathrm{J\,kg^{-1}}$). When the opposite occurs, part of the sweat drips off the body and does not contribute to the energy loss. Thereafter, the potential evaporation of sweat expresses the corresponding evaporative energy loss:

$$E_{\mathrm{sw}} = h_{\mathrm{e}} \cdot (\mathrm{VP_a} - \mathrm{SVP_{Tsk}}) \cdot A_{\mathrm{Du}} \quad (7)$$

where $\mathrm{VP_a}$ is the ambient water vapor pressure (in mb), $\mathrm{SVP_{Tsk}}$ is the saturation vapor pressure at the skin temperature (in mb), and h_{e} is the latent heat transfer coefficient (in $\mathrm{W\,m^{-2}\,mb^{-1}}$). Further, the skin wettedness is predicted as the ratio of the actual sweat rate to the potentially evaporating amount of sweat.

The aforementioned system of equations (1 to 3) comprises four unknown quantities, i.e., mean skin temperature, body core temperature, clothing surface temperature, and the storage flow of sensible energy in the body tissue, when the meteorological parameters, i.e., air temperature, vapor pressure, air velocity, and mean radiant temperature as well as the personal parameters, i.e., age, sex, height, weight, activity, mechanical efficiency, and body position, are defined. Thus, in order to solve this system of equations, initial values are required for the body temperatures. These values can be calculated from steady-state models. Since the initial values of mean skin temperature and body core temperature are defined, the storage flow of sensible energy in the body tissue can be evaluated, and through numerical integration over time steps, it is possible to compute the alterations in body temperatures. These new body

temperatures constitute the starting values for the next time step. Thus, the thermal state of the human body, characterized by the energy fluxes, the body temperatures, and the sweat rate, can be evaluated.

Simulation scenarios

The indoor setting utilized in the present analysis assumes a typical indoor environment, with climatic conditions of air temperature 23 °C, relative humidity 50 %, air speed 0.1 ms^{-1} and mean radiant temperature that equals the air temperature. In this environment, an "average" male individual 30 years old, weighting 70 kg, 1.75-m tall, and 1.8-m^2 body surface (ISO 8996 2004) has been considered, with a residency of more than an hour in the space. During this period, the model subject performed sedentary activity, and the assumed work metabolism was 80 W. According to this kind of activity, the mechanical efficiency was set at 0 %. Thus, the metabolic rate was equal to the rate of heat production (ISO 8996 2004). A summer clothing ensemble was considered to be worn by the model subject. The ensemble consisted of straight trousers, T-shirt, socks, and shoes, briefs included. Thus, the provided clothing insulation was 0.4 clo (ASHRAE 2004). Further, it was assumed that the climatic conditions as well as the physical activity and the clothing insulation did not display substantial differences during the stay of the model subject in the space. Thus, steady-state conditions formed under this typical indoor environment.

In order to compute the steady-state body temperatures of the model subject at the indoor setting, the stationary Munich Energy Balance Model for Individuals (MEMI) (Höppe 1993) has been employed. Thus, the mean skin temperature and the body core temperature of the model subject were formed at 33.5 and 36.9 °C, respectively. These body temperatures constituted the starting values at the moment of the model subject's transition from the indoor to the outdoor environment.

Three different, common in real-life scenarios have been considered for the model subject coming from the aforementioned indoor environment: (1) seating quite under tree shade conditions (scenario A); (2) seating quite under the sun (scenario B); and (3) walking under the sun (scenario C). In the first two scenarios, it was assumed that the model subject performed sedentary activity, and the work metabolism was 80 W. In the third one, it was assumed that the model subject walked on the level at a speed of 3.5 to 5.5 km h^{-1}, and the work metabolism was 190 W. Due to the light type of activity in the first two scenarios and the fact that the model subject walked on the level at the third one, the mechanical efficiency was set at 0 % (Fanger 1972; ISO 8996 2004). The time period of simulations has been set at 30 min, with a time step of 1 min, for each scenario. This selection was based on the fact that for a person leaving a neutral indoor climate and walking slowly under hot conditions, steady state of mean skin and body core temperature is reached after half and 1 h, respectively (Höppe 2002). Additionally, steady-state models cannot provide sufficient information for persons staying outdoors for less than half an hour (Höppe 2002), while thermal sensation can take at least half an hour to reach a steady-state condition (Jones and Ogawa 1992). A summary with the basic information for each scenario is given in Table 1.

Outdoor climatic conditions

The meteorological parameters used in these simulations were collected at the suburban area of the Athens University Campus, Greece, during a research campaign in July 2008. In particular, the meteorological data of ten experimental days with clear sky conditions at 14:00 summer local time (SLT) have been employed (Table 2). Thus, the entries in Table 2 constitute the climatic conditions at the outdoor setting where the model subject entered, coming from the indoor environment for each scenario.

Mean radiant temperature was modeled employing RayMan model (Matzarakis et al. 2007, 2010), according to climatic conditions as well as the suburban landscape and terrain of the greater experimental site. Further, the Bowen ratio was set at 1, the albedo of the surroundings was set at 0.18, while the albedo of human was set at 0.30.

Simulation results

Body parameters

Mean skin temperature

In the model subject coming from the same indoor environment, the starting value of mean skin temperature (T_{sk}) is formed at 33.5 °C for each scenario. From that minute onwards, T_{sk} reveals an increasing course on each experimental day with the temporal pattern of T_{sk} for three different air temperature (T_a) levels presented in Fig. 1a, b, c. An intense increasing trend of T_{sk} is noted during the first 6 to 10 min before the initial stabilization of the values, irrespectively of the scenario. At this time, the increasing gradient shows a similar form between scenarios B and C. On the other hand, the increasing trend reveals a lower gradient under tree shade conditions (scenario A) compared to the scenarios where the model subject is exposed under a higher radiation field (scenarios B and C). Further, it is noted that the increasing gradient is more intense at higher T_a levels, irrespectively of the scenario. Therefore, at a higher T_a (day 2, 37.6 °C), the increment of T_{sk} reaches up to 2.9, 3.8, and 3.8 °C during the first 10 min for scenarios A, B, and C, respectively. On the contrary, under lower T_a conditions

Table 1 Summary with the basic information for each scenario

	Model subject activity	Body position	Time period	Clothing insulation (clo)	Work metabolism (W)	Mechanical efficiency (%)
Indoor Setting	Performs sedentary activity	Sitting	More than an hour	0.4	80	0
Outdoor Setting						
Scenario A	Seat quite under tree shade conditions	Sitting	30 min	0.4	80	0
Scenario B	Seat quite under the sun	Sitting	30 min	0.4	80	0
Scenario C	Walk under the sun	Standing	30 min	0.4	190	0

(day 9, 28.1 °C), the first stabilization of the values occurs earlier (6 to 8 min) and the increment reaches up to 2.1, 3.4, and 3.4 °C for scenarios A, B, and C, respectively.

After the initial intense increasing trend, T_{sk} becomes stabilized for scenario A. From that minute onwards, the observed further increment of T_{sk} is up to 0.1 °C for each T_a level. For scenario B, T_{sk} is also stabilized with a further increment up to 0.1 °C, with the exception of the day with the highest T_a (day 2, 37.6 °C), where the increment reaches up to 0.4 °C. On the contrary, for scenario C, T_{sk} reveals a rough stabilization since a further increment varying between 0.2 °C at a lower T_a (day 9, 28.1 °C) up to 1.0 °C at a higher T_a (day 2, 37.6 °C) is observed.

It is worth noting that in scenarios B and C under the higher T_a conditions (day 2, 37.6 °C), T_{sk} presents an overshoot between the sixth and the tenth minute. That behavior of T_{sk} can be explained by the fact that sweating is not yet fully efficient at this moment. Similar behavior and course of T_{sk} have been observed in simulation (Höppe 2002) and experimental results (e.g., Katavoutas et al. 2009).

Mean skin temperature difference (ΔT_{sk}) between the initial (first minute) and the final (30th minute) value of T_{sk} versus T_a holds a positive sign for each scenario, as illustrated in Fig. 2a. Within the studied air temperature range, T_a increment of about 10 °C results in an increase of ΔT_{sk} by 1.0, 1.2, and 1.5 °C in scenarios A, B, and C, respectively. The relationship between ΔT_{sk} versus T_a is well-fitted by a linear equation with a high coefficient of determination (R^2_A=0.91) at the confidence level (c.l.) of 95 % for scenario A. Lower coefficient values are observed for scenarios B (R^2_B=0.64) and C (R^2_C=0.47) implying that further parameters trigger T_{sk}, such as direct solar radiation and higher work metabolism.

Body core temperature

In an effort to compare the potential health risks for the model subject, a comparison of the simulated body core temperature (T_c) for each scenario and for three different T_a levels is carried out (Fig. 1d, e, f). The temporal pattern of T_c reveals an increasing trend for scenarios B and C, independently of the T_a level. Moreover, higher T_c values are observed in scenario C, being explained by the higher work metabolism, as compared to the corresponding values in scenario B. On the contrary, in scenario A, T_c implies a rough stabilization of the values under the lower T_a levels (less than 32 °C) and a slightly increasing trend under the higher T_a conditions (more than 32 °C).

For an overall view, the scattered plot of the body core temperature difference (ΔT_c) versus T_a is shown in Fig. 2b. A visual inspection of the results implies a negative or no change of ΔT_c for T_a less than 32 °C and a positive ΔT_c up to 0.2 °C for T_a higher than 32 °C in scenario A. The relationship between ΔT_c and T_a is well-fitted by a linear equation with a high coefficient of determination (R^2_A=0.83, c.l. 95 %). On the other hand, ΔT_c is situated at higher values for scenario B with the difference ranging between 0.2 and 0.9 °C. Higher

Table 2 Meteorological parameters employed in the simulations

	Day 1	Day 2	Day 3	Day 4	Day 5	Day 6	Day 7	Day 8	Day 9	Day 10
Air temperature (°C)	35.2	37.6	28.4	30.4	31.4	36.3	35.5	33.4	28.1	29.0
Relative humidity (%)	42.1	15.7	28.7	26.7	28.8	20.2	24.7	22.4	28.3	30.8
Vapor pressure (hPa)	23.9	10.1	11.1	11.6	13.2	12.2	14.2	11.5	10.7	12.3
Air velocity (ms^{-1})	1.0	0.2	2.1	1.5	1.1	1.1	1.6	1.8	0.6	0.5
Air pressure (hPa)	989	985	984	984	984	984	980	976	979	979
Global radiation (Wm^{-2})	903	868	939	922	900	920	868	932	941	930
Mean radiant temperature in sun (°C)	63.3	66.3	56.4	58.6	59.8	64.2	61.0	60.8	60.4	61.3
Mean radiant temperature in shade (°C)	38.9	39.9	32.4	34.2	35.1	39.5	38.4	36.9	32.3	33.3

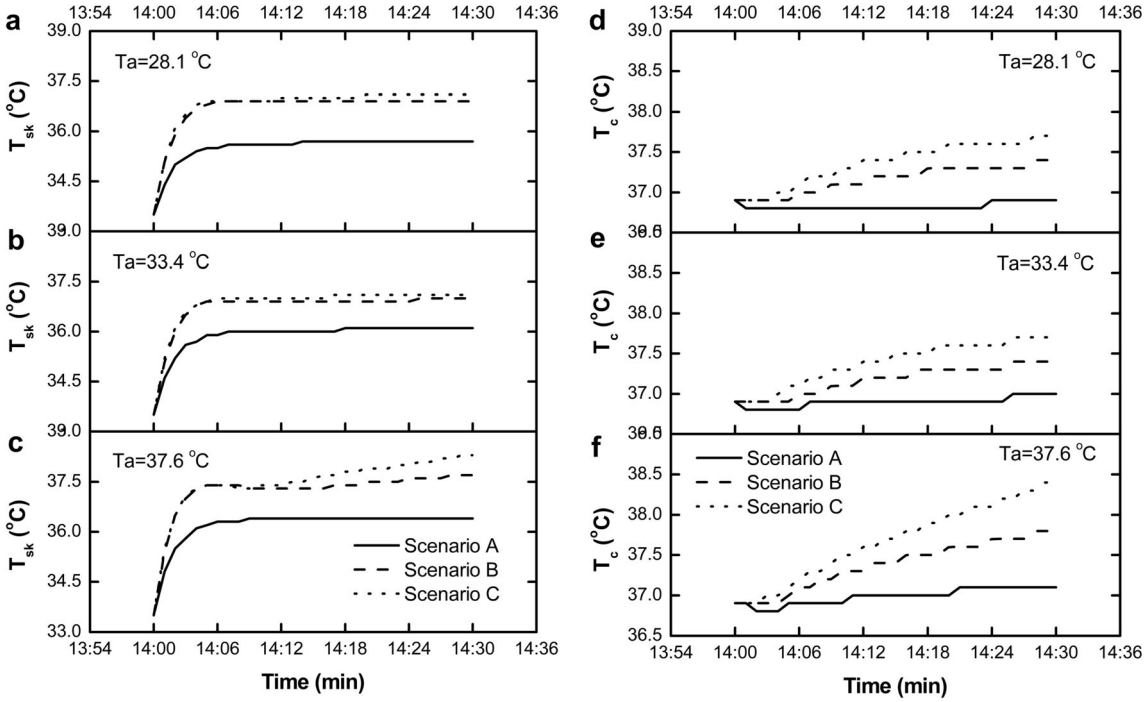

Fig. 1 Temporal courses of mean skin temperature (T_{sk}) (*left panel*) and body core temperature (T_c) (*right panel*) for each scenario after the transition from an indoor to three different outdoor environmental conditions **a**, **d** day 9; **b**, **e** day **8**; and **c**, **f** day 2

ΔT_c values are noted in scenario C, ranging from 0.6 to 1.5 °C. The lower coefficient values in scenarios B (R^2_B= 0.50) and C (R^2_C=0.46) as well as the higher ΔT_c values are attributed to the exposition of the model subject to the direct solar radiation (scenarios B and C) and the higher work metabolism (scenario C).

Clothing surface temperature

The relationship between initial (first minute) and final (30th minute) clothing surface temperature (T_{cl}) versus T_a is shown in Fig. 3. A visual inspection of the results indicates that final T_{cl} is formed at higher values compared to the corresponding initial T_{cl} values for each scenario. Further, initial T_{cl} varies at lower values (32.6–36.0 °C) for scenario A compared to the corresponding values for scenarios B (36.7–41.8 °C) and C (37.0–42.1 °C). Thus, T_a increment of about 10 °C results in an increase of initial T_{cl} by 3.4, 5.1, and 5.1 °C for scenarios A, B, and C, respectively, within the studied air temperature range. The final T_{cl} is also lower (33.2–37.2 °C) in scenario A compared to the corresponding values in scenarios B (37.7–43.5 °C) and C (38.1–44.1 °C). Therefore, a T_a increment of about 10 °C results in an increase of final T_{cl} by 4.0, 5.8, and 6.0 °C for scenarios A, B, and C, respectively.

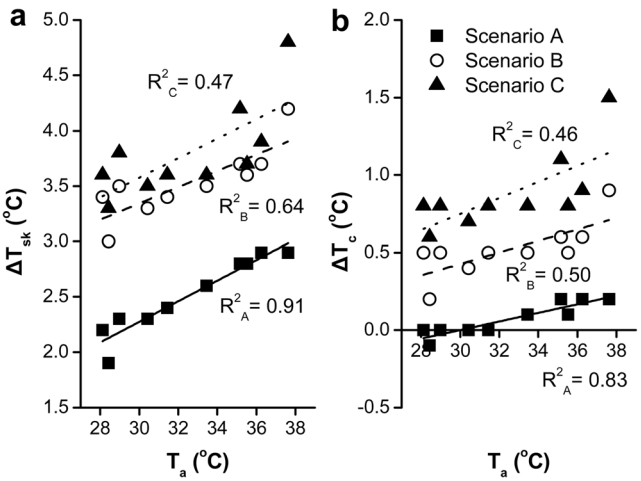

Fig. 2 Scatter plot of difference of **a** mean skin temperature (ΔT_{sk}) and **b** body core temperature (ΔT_c) versus air temperature (T_a) for each scenario. The regression lines are also illustrated

The relationship between initial and final T_{cl} versus T_a, through linear fit, indicates a high coefficient of determination (R^2_A=0.97 and 0.95, c.l. 95 %) in scenario A and lower coefficients in scenarios B and C ($R^2_{B/C}$=0.67 and 0.63, c.l. 95 %).

Additionally, the temporal pattern of T_{cl} for three different air temperature levels is shown in Fig. 4. A visual inspection of the results reveals an increasing trend of T_{cl} during the first 5 to 9 min. The overall study of all days (not shown) indicates that the rate of increment is higher in scenario C compared to the rate in scenario A, with a time lag between 1 and 4 min. This result essentially relates to the corresponding increasing trend and time lag of T_{sk} between the scenarios. After the first minutes of increasing trend, T_{cl} displays stabilization, with a further slight increase not exceeding 0.1 and 0.2 °C in scenarios A and B, respectively. On the other hand, in scenario C, a

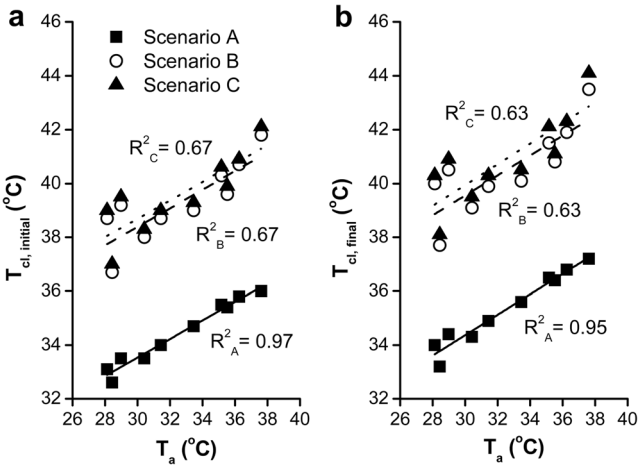

Fig. 3 Scatter plot of **a** initial (first minute) and **b** final (30th minute) clothing surface temperature (T_{cl}) versus air temperature (T_a) for each scenario. The regression lines are also illustrated

further increment is observed on each experimental day, and it fluctuates between 0.1 and 0.6 °C.

It is worth noting that in scenarios B and C at the higher air temperature (day 2, 37.6 °C), T_{cl} presents the same slight overshoot between the sixth and the tenth minute, as that observed for T_{sk}, as a result of the not yet fully efficient sweating at this moment.

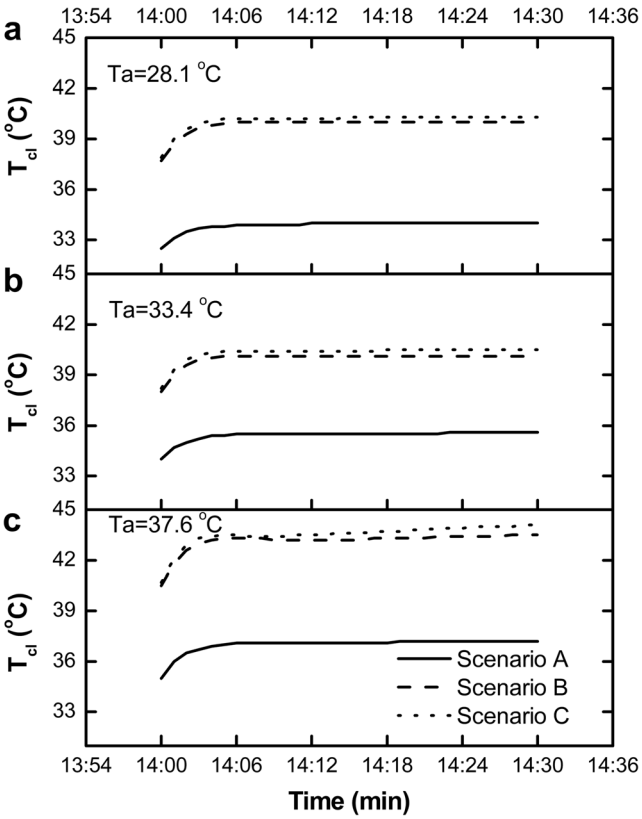

Fig. 4 Temporal courses of clothing surface temperature (T_{cl}) for each scenario after the transition from an indoor to three different outdoor environmental conditions **a** day 9, **b** day 8, and **c** day 2

Skin wettedness and water loss

One of the factors related to thermal discomfort in warm environments or during exercise is the level of wettedness over the skin surface, which constitutes the widely known index of skin wettedness (Gagge 1937) that could eventually predict thermal comfort (Havenith et al. 2002; Fukazawa and Havenith 2009). In an effort to investigate the level of skin wettedness of the whole body (w) per minute, a Box and Whisker plot is carried out, among the scenarios considered (Fig. 5a). In scenario A, a visual inspection of the results indicates that the 50 % of all data range between 10 and 20 % of w. The overall range, including the lower and upper bounds, reaches up to 30 %, and only the mild and extreme outliers exceed that value. On the other hand, in scenario B and C, all critical levels of w increase and an extensive dispersion of the values is observed. Therefore, the interquartile range increases significantly, lying between 30 and 60 % in scenario B. Further increment and dispersion are noted for the

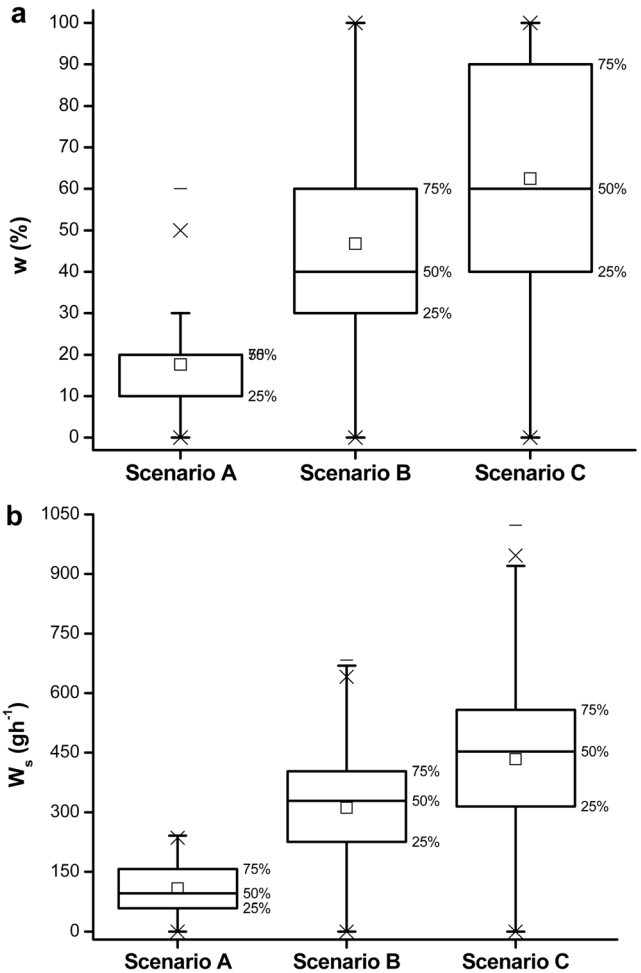

Fig. 5 Box and Whisker plot showing **a** skin wettedness (w) and **b** water loss (W_s) during the 30-min exposure for all days and scenarios. Inside the box, the *horizontal line* indicates the median, the *square* indicates the average, the *box* covers the 25–75 % percentiles, and the maximum length of each whisker is 1.5 times the interquartile range. *Points* outside this show up as mild and extreme outliers

interquartile range in scenario C, which fluctuates between 40 and 90 %, indicating the influence of radiation and activity.

According to the obtained results, the upper quartile (75 %) in scenario A is less than the range between 22 and 30 %, which constitutes the comfort limit of *w* for the whole body at rest (Nishi and Gagge 1977; Takanokura 1997). Thus, only the mild and extreme outliers, as well as a part of the upper bound (vertical bar outside the box), exceed the above range of comfort limit. However, in scenario B, the lower quartile (25 %) exceeds that range, and only a part of the lower bound (vertical bar outside the box) is less than that. On the other hand, in scenario C, the lower quartile (25 %) exceeds 36 %, which constitutes the comfort limit due to higher activity (Nishi and Gagge 1977; Fukazawa and Havenith 2009). Thus, only a part of the lower bound (vertical bar outside the box) is less than 36 %.

Additionally, a Box and Whisker plot of the water loss (Ws) per minute is carried out, among the scenarios considered (Fig. 5b). A visual inspection of the results reveals a limited dispersion of Ws (0 to 241.5 gh^{-1}) in scenario A, including the mild and extremes outliers, compared to the other two scenarios. On the contrary, in scenario B, the overall range of Ws is almost tripled (exceeds 683 gh^{-1}), with the interquartile ranging between 226.3 and 403.0 gh^{-1}. Further increment is noted for all critical levels of Ws in scenario C. In particular, the interquartile ranges between 316.6 and 557.6 gh^{-1}, while the extreme outliers reach up to 1,023 gh^{-1}. As the model subject is coming from the same indoor environment with no water loss, the above results reveal that the temporal pattern of Ws is steeper in scenario C compared to scenario B and in scenario B in comparison with A, as all critical levels of Ws increase per scenario.

Finally, Fig. 6 illustrates the relationship of average skin wettedness (*w*) versus air temperature (T_a) and air velocity (*v*).

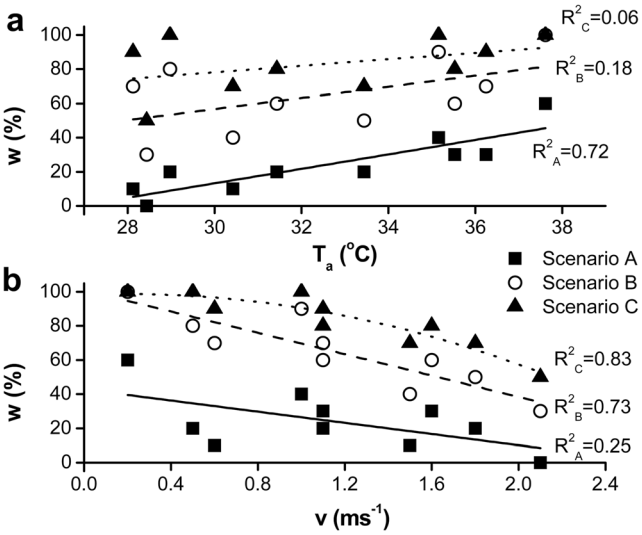

Fig. 6 Scatter plot of average skin wettedness versus **a** air temperature (T_a) and **b** air velocity (*v*) for each scenario. The regression lines are also illustrated

In scenario A, the relationship between *w* and T_a is well-fitted by a linear equation with a relatively high coefficient of determination (R^2_A=0.72, c.l. 95 %). Similar behavior under non-steady-state conditions in shade has also been observed in simulation results (Katavoutas et al. 2012). However, the results in scenarios B and C do not linearly fit well between *w* and T_a, displaying a low coefficient of determination. The pattern of the results is reversed when examining the relationship of *w* versus *v*. Consequently, a low coefficient is observed in scenario A and a relatively high coefficient is noted in scenarios B (R^2_B=0.73, c.l. 95 %), by a linear equation, and *C* (R^2_C=0.83, c.l. 95 %), by a polynomial equation. This inverted behavior is attributed to the cooling effect of *v* combined with high wettedness level over the skin surface (*w*), as seen in scenarios B and C. On the contrary, the cooling effect of *v* is reduced in scenario A, due to the low *w* levels, while T_a seems to have greater influence on w.

Human energy fluxes

To assess the magnitude of the formed energy balance, the average energy fluxes have been calculated, per scenario, from lower to higher air temperature values (Fig. 7). The range of average energy gains and losses is sub twofold in scenario A (−140 to 192 W) compared to scenario B (−274 to 433 W) and almost sub threefold in comparison with scenario C (−338 to 551 W).

Due to the same kind of activity and the same mechanical efficiency, the average internal energy production (H) is formed at 162.7 W in scenarios A and B. On the contrary, H is formed at 272.7 W due to the higher activity in scenario C.

The average radiative energy (RN) presents decreasing marginal losses at lower air temperature values and increasing gains at higher air temperature values, as air temperature increases in scenario A. These marginal losses of RN are attributed to the higher surface temperature of the body (T_{sk} and T_{cl}) from the formable T_{mrt} under tree shade conditions. The average RN increases significantly (at least 204 W) in scenarios B and C, due to the exposure of the subject to the direct solar radiation. The marginal RN differences between scenarios B and C are attributed to the different body position.

The average convective energy (*C*) reveals a decreasing loss as air temperature increases for each scenario. This reduction of the loss is associated with the decreasing gradient between the air temperature and the surface temperature of the body (T_{sk} and T_{cl}). Thus, the rate of increment of T_{sk} is lower, compared to the corresponding increase of air temperature, due to the process of sweating, resulting in the reduction of average convective energy loss. However, these losses are smaller in scenario A (at least 20 W) compared to the losses at the other two scenarios, where the differences between them are marginal. This result is attributed to the lower T_{sk} in scenario A, due to the shade conditions and the light kind of

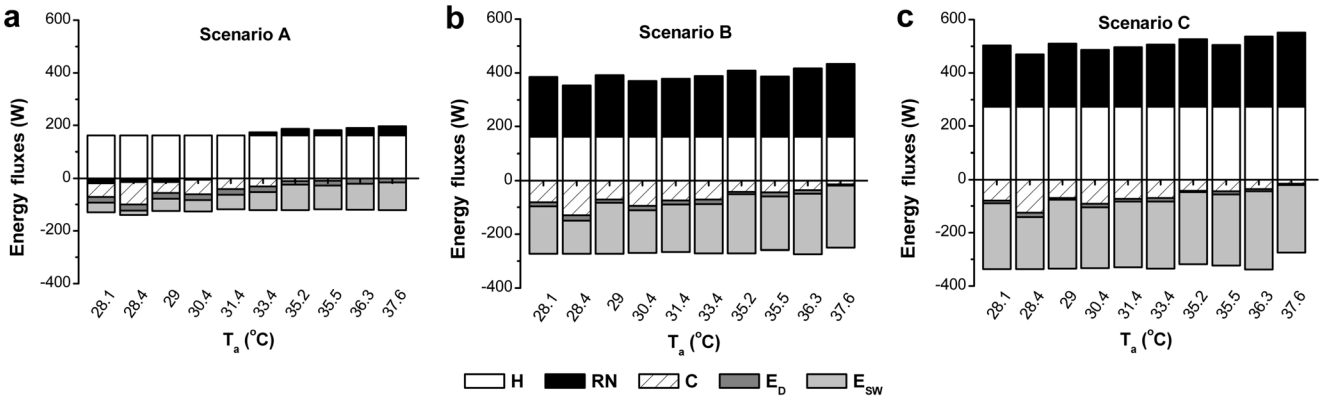

Fig. 7 Average human energy fluxes versus air temperature (T_a) for each scenario (*H* internal energy production, *RN* radiative energy, *C* convective energy, E_D energy loss by skin diffusion, E_{sw} evaporative energy loss of sweat)

activity, in comparison with the formed T_{sk} at the other two scenarios.

The average energy loss by skin diffusion (E_D) presents the lowest range among the other energy fluxes, with the exception of average RN in scenario A. Thus, average E_D displays the higher losses in scenario A (up to −23 W) compared to the losses in scenarios B (up to −20 W) and C (up to −17 W). That result is attributed to the lower T_{sk} values in scenario A.

Finally, the average evaporative energy loss of sweat (E_{sw}) indicates higher losses at least two and half times in scenario C compared to the corresponding losses in scenario A. It is worth noting that this ratio is higher at lower air temperature values, reaching up to almost 12 times higher loss in the case with the highest air velocity (2.1 ms^{-1}). The maximum average E_{SW} does not exceed −106 W in scenario A, at least sub twofold compared to the maximum loss in scenario B (−231 W) and almost sub threefold in comparison with the maximum loss in scenario C (−293 W).

Convective energy flux

The temporal variation of C reveals a similar pattern for each scenario, displaying an inverse form of T_{sk} and T_{cl}, as indicatively presented for three different T_a conditions (Fig. 8). Thus, an intense increasing loss of *C* is noted in the first 6 to 10 min of each experimental day in scenarios B and C. A similar intense increasing loss is observed in scenario A, for the lower air temperature values. However, the fact that *C* presents a decreasing loss as air temperature increases results to an intense decreasing gain for higher air temperature values. After the initial intense trend, *C* has been almost stabilized for each scenario, keeping up with the corresponding stabilization of T_{sk} and T_{cl}.

Evaporative energy flux

The model subject coming from the same neutral indoor environment, the starting value of E_{sw} is nil due to the absence of perspiration on each scenario at this time (Fig. 9a, b, c). From that minute onwards, E_{sw} reveals an increasing loss on each experimental day, with the steepest gradient formed in scenario *C* compared to the other two scenarios and in scenario B in comparison with A. Consequently, the increasing loss in scenario B is placed between the other two scenarios, which is explained by the fact that this case combines the effect of light kind of activity and the effect of direct solar radiation. The increasing loss of E_{sw}, at the higher air temperature (day 2, 37.6 °C), presents a kind of stabilization from the

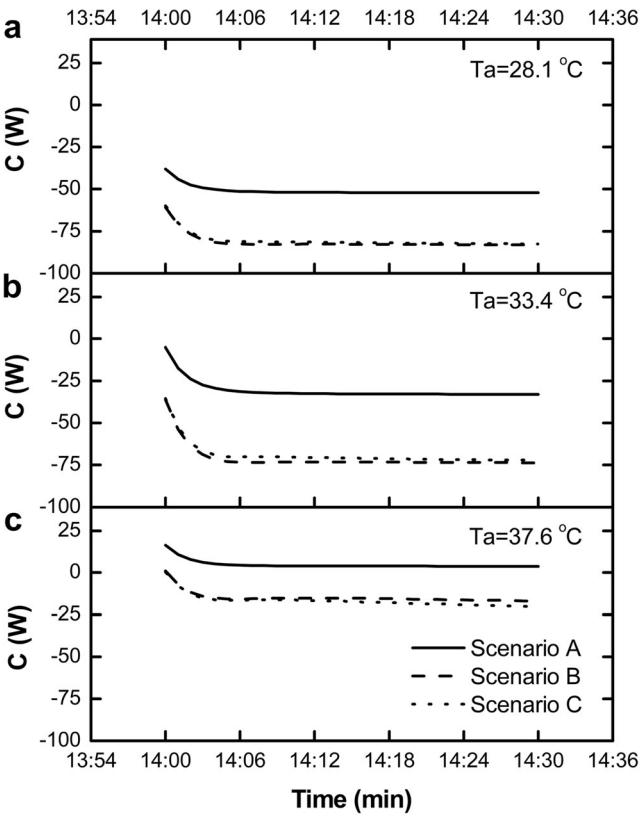

Fig. 8 Temporal courses of convective energy flux (*C*) for each scenario after the transition from an indoor to three different outdoor environmental conditions **a** day 9, **b** day 8, and **c** day 2

16th and 11th minute onwards in scenarios B and C, respectively. This result is attributed to the overall coverage of the skin surface with sweat, reaching at this time the maximum value of skin wettedness (100 %). Thus, a part of the sweat is dripping off the body, leading to the observed intense reduction of the energy loss rate, as the amount of sweat produced from the body is higher than the potential evaporation (Höppe 1993). The above result is not observed in scenario A. In scenario B, it is noted only on the day with the higher air temperature (day 2, 37.6 °C), 16 min after leaving the indoor environment. Finally, in scenario C, it is observed in three cases, the day with the higher air temperature (day 2), the day with high air temperature and the higher relative humidity (day 1), and the day with relatively high relative humidity and low wind speed (day 10). It is worth noting, that the occurrence time of the intense reduction of energy loss rate is differentiated among the 3 days. Thus, it is observed 11 (day 2), 16 (day1), and 24 (day 10)min after the transition from the indoor to the outdoor environment.

Energy flux by skin diffusion

The temporal pattern of E_D indicates a decreasing loss for each scenario, with the lower gradient being observed in scenario A and the higher in scenario C, as indicatively presented for three different T_a conditions (Fig. 9d, e, f). However, in the first 3 min, a marginal increasing loss is noted in scenario A. At this time, T_{sk} increases and the skin wettedness is nil. Gradually, the water loss by diffusion cannot be performed from fully moistened skin portions due to the sweat formation and the skin wettedness increment. Thus, a conversion of E_D gradient is observed. The above result is not observed in scenario C and marginally is noted in scenario B, due to the higher sweat formation and the higher level of wettedness over the skin surface from the first minutes. Further, at the higher T_a (day 2, 37.6 °C), E_D is nil after 11 and 16 min in the outdoor environment for scenarios C and B, respectively. From the above minutes onwards, skin wettedness is formed at the maximum value (100 %), and the skin surface of the body is fully moistened, preventing the diffusion through the skin. The above result is not observed in scenario A in any experimental day. On the contrary, it is observed the same days at the same minute as in the case of the intense reduction of energy loss E_{sw} rate in scenarios B and C. Consequently, the water loss observed at this time is coming completely from sweating.

Discussion and conclusions

The simulations conducted with the dynamic two-node IMEM model have shown that the adaptation and the response of a person, coming from the same neutral indoor climate, vary depending on the scenario followed by the individual while being outdoors. The combination of radiation field

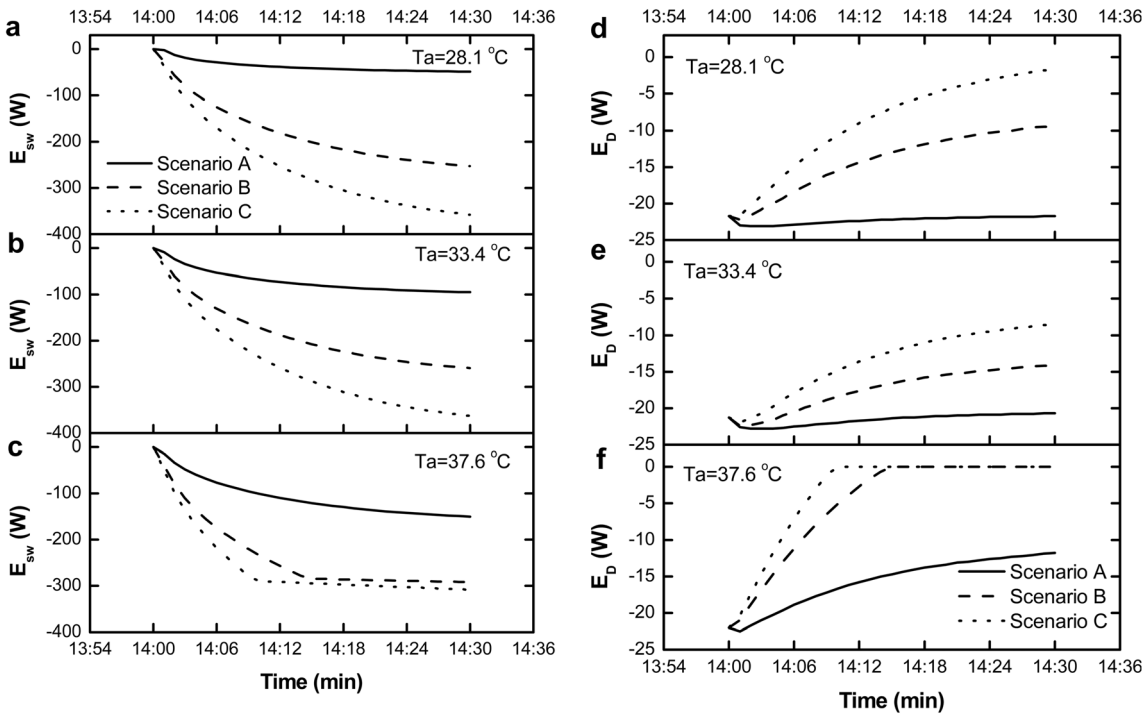

Fig. 9 Temporal courses of evaporative energy flux (E_{sw}) (*left panel*) and energy flux by skin diffusion (E_D) (*right panel*) for each scenario after the transition from an indoor to three different outdoor environmental conditions **a**, **d** day 9; **b**, **e** day 8; and **c**, **f** day 2

(shade or not) with the kind of activity (sitting or walking) and the outdoor climatic conditions differentiates significantly the thermal state of the human body.

The results for the mean skin temperature (T_{sk}) reveal an intense increasing trend the first minutes (up to the tenth minute) and a kind of stabilization thereafter. Similar behavior and course of T_{sk} have been observed in simulation (Höppe 2002) and experimental results (e.g., Katavoutas et al. 2009) as an outcome of the thermal adaptation process. The gradient of the increasing trend is lower for the sitting individual under the shade (scenario A) than under direct solar radiation for the sitting (scenario B) and for the walking subject (scenario C). The increment of T_{sk} is lower in scenario A than in scenarios B and C, after a 30-min exposure to the outdoor climatic conditions considered. On the other hand, body core temperature difference (ΔT_c) between the initial (first minute) and the final (30th minute) value of T_c indicates a positive sign for scenarios B and C. However, in scenario A, the results imply a negative or no change of ΔT_c for air temperature values less than 32 °C and a positive ΔT_c up to 0.2 °C for air temperature values higher than 32 °C. Such a behavior of ΔT_c for air temperature values higher and lower than 32 °C has also been observed for a person leaving an indoor environment and seating under tree shade conditions during hot summer days (Katavoutas et al. 2012). In every scenario, ΔT_c values are lower than the corresponding ΔT_{sk} values, which means that under hot conditions, the adaption rate of the core part of the human body is much slower than the adaptation rate of the skin part. This outcome has also been observed in the case of a pedestrian experiencing thermal transient (Höppe 2002; Chen and Ng 2011, 2012). The temporal course of clothing surface temperature (T_{cl}) reveals a similar pattern with T_{sk}. Initial (1st min) and final (30th min) T_{cl} values are at least 4 °C lower under the shade (scenario A) than under direct solar radiation for the sitting (scenario B) and for the walking subject (scenario C). Further, it is found that 75 % of the skin wettedness (w) values per minute do not exceed the thermal comfort limit at rest for the sitting individual under the shade (scenario A). The above percentage decreases dramatically for the sitting individual under direct solar radiation (scenario B), and it is less than 25 % of w. Although thermal comfort limit is higher for the person walking under direct solar radiation (scenario C), it is found that 75 % of w values exceed that thermal comfort limit. In the considered outdoor climatic conditions, the average range of the formed energy balance is sub twofold in scenario A than in scenario B and almost sub threefold in comparison with scenario C. Although the individual comes from the same indoor climate, the temporal patterns of human energy fluxes vary significantly, due to the scenario followed while being outdoors. Further, those patterns are stimulated by body temperatures and skin wettedness.

The previous analysis gives an insight on how to address the problem of non-steady-state conditions in thermal comfort via dynamic modeling. Although the thermophysiological parameters and the human energy fluxes might not be quite informative for those who are unfamiliar with this field of knowledge, they can give helpful and additional information. Since there is a lack of commonly accepted methodology for dynamic thermal assessment, these parameters sufficiently depict the effects of the thermal environment on the human body during thermal transients.

References

Al-Othmani M, Ghaddar N, Ghali K (2008) A multi-segmented human bioheat model for transient and asymmetric radiative environments. Int J Heat Mass Transfer 51:5522–5533

ASHRAE (2004) Thermal environmental conditions for human occupancy. ASHRAE standard 55, Atlanta

Brasche S, Bischof W (2005) Daily time spent indoors in German homes-baseline data for the assessment of indoor exposure of German occupants. Int J Hyg Environ Health 208:247–253

Chen L, Ng E (2011) Assessing pedestrian's thermal transient condition: a bottom-up simulation approach. In: Proceedings of 45th Annual Conference of the Architectural Science Association, ANZAScA, University of Sydney

Chen L, Ng E (2012) Computer simulation of pedestrian's transient thermal comfort in a complex urban context: a bottom-up modeling approach. In: proceedings of 7th Windsor Conference: the changing context of comfort in an unpredictable world. Cumberland Lodge, Windsor

Chun C, Tamura A (2005) Thermal comfort in urban transitional spaces. Build Environ 40:633–639

de Dear RJ, Ring JW, Fanger PO (1993) Thermal sensations resulting from sudden ambient temperature changes. Indoor Air 3:181–192

Fanger PO (1972) Thermal comfort. McGraw Hill, New York

Fiala D, Lomas KJ, Stohrer M (2001) Computer prediction of human thermoregulatory and temperature responses to a wide range of environmental conditions. Int J Biometeorol 45:143–159

Foda E, Sirén K (2011) A new approach using the pierce two-node model for different body parts. Int J Biometeorol 55:519–532

Fukazawa T, Havenith G (2009) Differences in comfort perception in relation to local and whole body skin wettedness. Eur J Appl Physiol 106:15–24

Gagge AP (1937) A new physiological variable associated with sensible and insensible perspiration. Am J Physiol 120:227–287

Gagge AP, Stolwijk JAJ, Nishi Y (1971) An effective temperature scale based on a simple model of human physiological regulatory response. ASHRAE Trans 77:247–262

Havenith G, Holmer I, Parsons K (2002) Personal factors in thermal comfort assessment: clothing properties and metabolic heat production. Energy Build 34:581–591

Höppe P (1984) Die Energiebilanz des Menschen. Dissertation, Universität München–Meteorologisches Institut

Höppe P (1989) Application of a dynamical energy balance model for the prediction of thermal sensation and comfort. In: Driscoll D, Box EO (eds) Proc. of the 11th ISB-Congress. West Lafayette, USA, pp 267–272

Höppe PR (1993) Heat balance modelling. Experientia 49:741–746

Höppe P (1997) Aspects of human biometeorology in past, present and future. Int J Biometeorol 40:19–23

Höppe P (1999) The physiological equivalent temperature-a universal index for the biometeorological assessment of the thermal environment. Int J Biometeorol 43:71–75

Höppe P (2002) Different aspects of assessing indoor and outdoor thermal comfort. Energy Build 34:661–665

Huizenga C, Hui Z, Arens E (2001) A model of human physiology and comfort for assessing complex thermal environments. Build Environ 36:691–699

ISO 8996 (2004) Ergonomics of the thermal environment—determination of metabolic rate. Int organ stand Geneva

Jones BW, Ogawa Y (1992) Transient interaction between the human and the thermal environment. ASHRAE Trans 98:189–195

Katavoutas G, Theoharatos G, Flocas HA, Asimakopoulos DN (2009) Measuring the effects of heat wave episodes on the human body's thermal balance. Int J Biometeorol 53:177–187

Katavoutas G, Flocas HA, Tsitsomitsiou M (2012) Thermal comfort in hot outdoor environment under unsteady conditions. In: Helmis CG, Nastos PT (eds) Advances in meteorology, climatology and atmospheric physics. Springer, Verlag Berlin Heidelberg, Vol. 1, pp 175–180

Leech JA, Nelson WC, Burnett RT, Aaron S, Raizenne ME (2002) It's about time: a comparison of Canadian and American time-activity patterns. J Expo Anal Environ Epidemiol 12:427–432

Matzarakis A, Rutz F, Mayer H (2007) Modelling radiation fluxes in simple and complex environments-application of the RayMan model. Int J Biometeorol 51:323–334

Matzarakis A, Rutz F, Mayer H (2010) Modelling radiation fluxes in simple and complex environments: basics of the RayMan model. Int J Biometeorol 54:131–139

Mayer H, Höppe P (1987) Thermal comfort of man in different urban environments. Theor Appl Climatol 38:43–49

Nishi Y, Gagge AP (1977) Effective temperature scale for use in hypo—and hyperbaric environments. Aviat Space Environ Med 48:97–107

Schappeler TE (2011) Development of an FEA-based whole-body human thermal model for evaluating blood cooling/warming techniques, ProQuest, UMI Dissertation Publishing

Spagnolo J, de Dear R (2003) A field study of thermal comfort in outdoor and semi-outdoor environments in subtropical Sydney Australia. Build Environ 38:721–738

Stolwijk JAJ (1971) A mathematical model of physiological temperature regulation in man. NASA, Washington DC, CR-1855

Takanokura M (1997) Effect of change in wettedness on wear comfort during exercise with sweating. Bull Showagakuin Jr Coll 33:63–72

Tanabe SI, Kobayashi K, Nakano J, Ozeki Y, Konishi M (2002) Evaluation of thermal comfort using combined multi-node thermoregulation (65MN) and radiation models and computational fluid dynamics (CFD). Energy Build 34:637–646

VDI (1998) Methoden zur human-biometeorologischen Bewertung von Klima und Lufthygiene für die Stadt-und Regionalplanung. Teil I: Klima.-VDI-Richtlinie 3787 Blatt2

Yi L, Fengzhi L, Yingxi L, Zhongxuan L (2004) An integrated model for simulating interactive thermal processes in human-clothing system. J Therm Biol 29:567–575

Zolfaghari A, Maerefat M (2010) A new simplified thermoregulatory bioheat model for evaluating thermal response of the human body to transient environments. Build Environ 45:2068–2076